Journal of Colloid and Interface Science 608 (2022) 1813–1826

Contents lists available at ScienceDirect

Journal of Colloid and Interface Science

journal homepage: www.elsevier.com/locate/jcis

Carbon nanogels exert multipronged attack on resistant bacteria and strongly constrain resistance evolution

Ju-Yi Mao [a], Dragan Miscevic [b], Binesh Unnikrishnan [a], Han-Wei Chu [a], C. Perry Chou [b], Lung Chang [c], Han-Jia Lin [a,d], Chih-Ching Huang [a,d,e,*]

[a] Department of Bioscience and Biotechnology, National Taiwan Ocean University, Keelung 202301, Taiwan, ROC
[b] Department of Chemical Engineering, University of Waterloo, 200 University Avenue West, Waterloo, ON N2L 3G1, Canada
[c] Department of Pediatrics, Mackay Memorial Hospital and Mackay Junior College of Medicine Nursing and Management, Taipei 10449, Taiwan
[d] Center of Excellence for the Oceans, National Taiwan Ocean University, Keelung 202301, Taiwan, ROC
[e] School of Pharmacy, College of Pharmacy, Kaohsiung Medical University, Kaohsiung 80708, Taiwan, ROC

HIGHLIGHTS

- Pyrolysis of L-lysine hydrochloride can form partially carbonized nanogels (CNGs).
- CNGs exhibit potent antibacterial activity against biopolymer-producing bacteria and antibiotic-resistant clinical isolates.
- CNGs suppress bacteria through multiple mechanisms, such as membrane disruption and oxidative stress elevation.
- In contrast to antibiotics and other nanomaterials, CNGs steadily treat bacteria even after acclimation for 20 passages.

GRAPHICAL ABSTRACT

Thermal transformation of amino acid to bio-carbonized nanogels: Exerting multiple modes of action to suppress drug-resistant bacteria, biopolymer-producing bacteria, and clinical isolates.

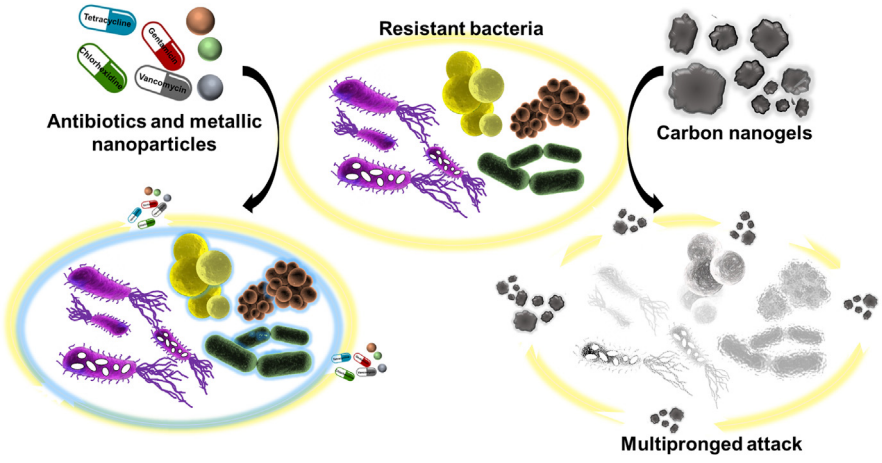

ARTICLE INFO

Article history:
Received 31 July 2021
Revised 16 October 2021
Accepted 18 October 2021
Available online 21 October 2021

Keywords:
Amino acids
Drug resistance
Carbon nanomaterials
Bacterial mutation
Antimicrobials

ABSTRACT

Developing antimicrobial agents that can eradicate drug-resistant (DR) bacteria and provide sustained protection from DR bacteria is a major challenge. Herein, we report a mild pyrolysis approach to prepare carbon nanogels (CNGs) through polymerization and the partial carbonization of L-lysine hydrochloride at 270 °C as a potential broad-spectrum antimicrobial agent that can inhibit biopolymer-producing bacteria and clinical drug-resistant isolates and tackle drug resistance issues. We thoroughly studied the structures of the CNGs, their antibacterial mechanism, and biocompatibility. CNGs possess superior bacteriostatic effects against drug-resistant bacteria compared to some commonly explored antibacterial nanomaterials (silver, copper oxide, and zinc oxide nanoparticles, and graphene oxide) through multiple antimicrobial mechanisms, including reactive oxygen species generation, membrane potential dissipation, and membrane function disruption, due to the positive charge and flexible colloidal structures resulting strong interaction with bacterial membrane. The minimum inhibitory concentration (MIC)

* Corresponding author at: Department of Bioscience and Biotechnology, National Taiwan Ocean University, Keelung 202301, Taiwan, ROC.
E-mail address: huanging@ntou.edu.tw (C.-C. Huang).

https://doi.org/10.1016/j.jcis.2021.10.107

values of the CNGs (0.6 μg mL^{-1} against *E. coli* and *S. aureus*) remained almost the same against the bacteria after 20 passages; however, the MIC values increased significantly after treatment with silver nanoparticles, antibiotics, the bacteriostatic chlorhexidine, and especially gentamicin (approximately 140-fold). Additionally, the CNGs showed a negligible MIC value difference against the obtained resistant bacteria after acclimation to the abovementioned antimicrobial agents. The findings of this study unveil the development of antimicrobial CNGs as a sustainable solution to combat multidrug-resistant bacteria.

1. Introduction

Most bacteria in severe conditions, such as those being treated long-term with antibiotics, can acquire special genes to increase their survival rate through horizontal gene transfer (HGT) or arose from a gene mutation, leading to the acquisition of drug resistance [1]. HGT occurs through multiple mechanisms and allows genetic material to transfer between bacterial strains and species (*e.g.*, biofilms and biopolymer-producing bacteria) [2]. Biopolymers produced by certain bacteria also provide increased resistance to environmental stress factors, including antimicrobial agents. Therefore, drug-resistant or biopolymer-producing genes may cause robust resistance to environmental stress [3–6]. For example, granules of polyhydroxyalkanoate biopolymers can provide improved cellular integrity when cells are exposed to sudden osmotic changes (200 g L^{-1} NaCl) in the environment [3]. These biopolymers can also block UV irradiation and provide increased UV resistance in polymer-rich bacterial strains, leading to a 3-fold increase in survival rate [4]. In addition, biopolymers can act as nutrient resources for bacteria under starvation conditions [5]. Some biopolymers produced by microorganisms have been found to have properties similar to those of plastic [7]; therefore, industrial production of biodegradable plastics through these biopolymer-producing microbes is of great commercial interest [8]. Tremendous research on biopolymer-producing bacteria is ongoing for the large-scale production of biopolymers and the modification of polymers for suitable applications [9–11]. These genetic materials (*e.g.*, biopolymer-producing genes or drug-

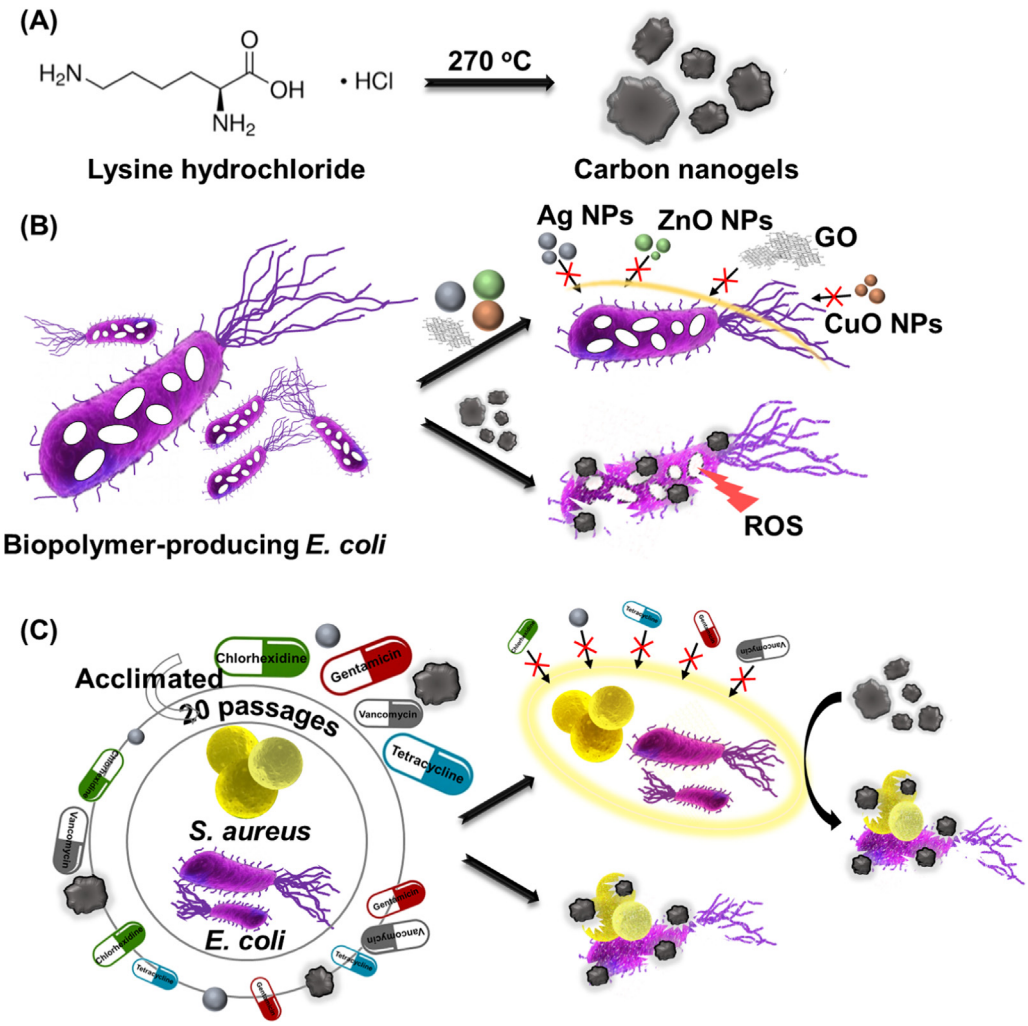

Scheme 1. Schematic representations of (A) the synthesis of the carbon nanogels (CNGs) by heat treatment of L-lysine hydrochloride; (B) the antibacterial action of CNGs on biopolymer-producing bacteria; (C) the antibacterial effects of CNGs against bacteria that developed drug resistance after acclimation for 20 passages with silver ions, silver nanoparticles, antibiotics, and CNGs.

resistant genes) transfer to pathogenic bacterial strains, which greatly exacerbate drug resistance and severely affect the environment [12]. Combined with the already present problem of multidrug resistance, the transfer of biopolymer-producing genes to pathogenic bacteria may cause environmental contamination resulting in epidemics and pose a major challenge in the future.

Many strategies have been employed to treat drug-resistant bacteria, including the development of new antibiotics, derivatives of existing antibiotics, antibiotic adjuvants, and peptide antibiotics from mammals and other organisms [13]. However, the bacteria that respond to these materials can still develop drug resistance over time. These methods are also generally expensive [14]. Nanomaterials are widely reported to exhibit antimicrobial properties that have been explored as next-generation nanomedicines to reduce drug resistance, including silver (Ag), copper oxide (CuO), iron oxide, titanium oxide, and zinc oxide (ZnO) nanoparticles (NPs) and carbon nanomaterials such as graphene oxide (GO) and carbon quantum dots [15–18]. However, recent studies have suggested that metal- or metal oxide-based antibacterial nanoparticles may also face drug resistance issues similar to those faced by conventional antibiotics [19]. Bacteria develop resistance to Ag NPs through repeated exposure by producing flagellin that disrupts the colloidal stability of Ag NPs and causes them to aggregate [20]. Additionally, Ag NPs are highly mutagenic toward *E. coli* upon repeated exposure, and the mutated strains have shown improved resistance to ampicillin [21]. Moreover, toxicity from the metal of these metallic NPs is a concern for practical applications. Carbon-based antibacterial nanomaterials (CNMs) have been recently considered a potential alternative to inorganic nanomaterials and antibiotics due to their high biocompatibility, varied functional properties, a wide choice of raw materials, and easy synthesis methods [22–25]. However, whether bacteria can develop resistance after long-term exposure to CNMs has yet to be tested. Therefore, at present, developing novel CNMs with broad-spectrum antimicrobial properties toward drug-resistant biopolymer-producing pathogens and clinical isolates through a detailed investigation of the ability of CNMs to suppress the development of drug resistance is highly desirable. Carbonized nanogels (CNGs) are a new category of carbon nanomaterials with carbonized nanostructures embedded in the polymer matrix [26]. Their properties highly vary depending upon their parent molecules and the synthesis methods. We reported the synthesis of CNGs from sodium alginate for anticoagulation application, and other CNGs from lysine and quercetin/lysine for antiviral and antibacterial applications [27–29]. CNGs synthesized from a mixture of quercetin and lysine are effective for the treatment of bacterial keratitis through simultaneous antibacterial and antioxidant effects [28]. Whereas CNGs synthesized from only lysine exhibit virus inhibition properties against Infectious Bronchitis Virus by inhibiting virus attachment to the host cells [29]. CNGs derived from different precursors enable different applications; however, their antibacterial potential has not been explored. Therefore, there is plenty of scope for further exploration of their antimicrobial applications. Herein, we conducted a thorough investigation of lysine-derived carbon nanogels (hereafter CNGs-270, where 270 represents synthesis temperature in degree Celsius) for antibacterial application and their ability to suppress bacterial drug resistance in *E coli*, *S. aureus*, drug-resistant bacteria, clinical isolates, and biopolymer [poly(3-hydroxybutyrate-*co*-3-hydroxyvalerate); PHBV]-producing *E. coli*. CNGs-270 exhibited a multifaceted attack on bacteria resulting in the suppression of drug-resistance evolution, which is illustrated in Scheme 1. The antibacterial drug resistance upon exposure to CNGs-270, Ag NPs, CuO NPs, and ZnO NPs, graphene oxide, and antibiotics were studied in various acclimated bacteria strains and the CNGs-270 were found to exhibit superior activity than the others.

2. Materials and methods

2.1. Materials

L-Lysine monohydrochloride (L-lysine·HCl), hydrochloric acid (HCl), sodium chloride (NaCl), potassium chloride (KCl), magnesium chloride ($MgCl_2$), calcium chloride ($CaCl_2$), poly-L-lysine, lysogeny broth LB-Lennox, tris(hydroxymethyl)aminomethane (Tris), copper(II) oxide nanoparticles, and zinc oxide nanoparticles were purchased from Sigma-Aldrich (St. Louis, MO, USA). The 2′,7′-dichlorodihydrofluorescein diacetate (DCFH-DA) was purchased from Invitrogen. Graphite powder (99%, 7–11 μm) for the synthesis of graphene oxide (GO) was obtained from Alfa Aesar (Heysham, Lancashire, UK). Phosphoric acid and acetic acid were purchased from Mallinckrodt Baker (Phillipsburg, NJ, USA). Potassium permanganate ($KMnO_4$), sulfuric acid (H_2SO_4), and hydrogen peroxide (H_2O_2) were obtained from SHOWA (Tokyo, Japan). All chemicals were used without purification. Phosphate-buffered saline (PBS; containing 137 mM NaCl, 2.7 mM KCl, 10 mM Na_2HPO_4, and 1.8 mM KH_2PO_4; pH 7.4) was used to mimic physiological conditions. Milli-Q ultrapure water (18.2 MΩ·cm; EMD Millipore, Billerica, MA, USA) was used in all experiments.

2.2. Synthesis of CNGs

Carbon nanogels (CNGs) were synthesized by the simple, controlled heating of L-lysine hydrochloride according to our previous work [29]. Briefly, 0.05 g of L-lysine hydrochloride was transferred to a 20 mL crucible and heated in a preheated oven at 180, 210, 240, 270, or 300 °C for 3 h. Then, the solid was cooled to room temperature, and 5 mL of deionized water was added. After sonication for 1 h, the mixture was centrifuged at a relative centrifugal force (RCF) of 5,000 *g* for 30 min. The solid residue was discarded, and the supernatant containing the CNG dispersion was collected and stored at − 20 °C. The CNG dispersions were purified by dialysis using a dialysis membrane (MWCO = 0.5–1.0 k_D; Float-A-Lyzer G2, Spectrum Laboratories, Rancho Dominguez, CA, USA) with deionized water (500 mL) that was replaced every 1 h for 5 h and then every 12 h for 24 h for further characterization. The CNG solution after dialysis was lyophilized to generate a dry powder before use.

2.3. Bacterial growth and MIC and MBC testing assays

All bacterial strains, including *E. coli* (BRBC 12438), *S. aureus* (BCRC10781), and biopolymer-producing *E. coli*, were grown separately in Lysogeny broth LB-Lennox media. Except for the wild-type strain, a single colony of PHBVΔ*sdhA E. coli* was inoculated in LB medium with glucose (20 g L^{-1}) for high biopolymer content induction. The cultures were incubated at 37 °C with shaking until the absorbance at 600 nm (OD_{600}) reached 1.0 (optical path length = 1.0 cm). A total of 1.0 mL of each cell mixture was centrifuged at 3,000 *g* for 10 min at 25 °C and washed three times with 1.0 mL of sodium phosphate buffer (5 mM, pH 7.4) for experiments. The minimal inhibition concentrations (MICs) of the CNGs and other materials against the tested bacterial strains were determined using the broth microdilution and agar-plate method. Briefly, all bacteria (1×10^4 CFU mL^{-1}) were incubated with CNGs or nanomaterials (0.1–100 μg mL^{-1}) for 3 h in sodium phosphate buffer (5 mM, pH 7.4) at 25 °C with shaking. Then, 50 μL of each suspension was spread on LB agar plates and incubated overnight at 37 °C. The MIC value is reported as the lowest concentration of CNGs or other materials capable of > 90% inhibition of bacterial growth compared to the control group. The minimum bactericidal

concentration (MBC) value was determined as the lowest concentration of each nanomaterial needed to kill a particular bacterium.

2.4. Bacterial TEM images

Bacterial suspensions of the wild-type and biopolymer-producing *E. coli* (10^9 CFU mL^{-1}, 1 mL) were centrifuged (RCF 3,500 *g*, 10 min, 25 °C) and washed with 1 mL of sodium phosphate buffer (5 mM, pH 7.4) three times. Then, 50 μL of each *E. coli* suspension (10^8 CFU mL^{-1}) was incubated with CNGs-270 (100 μg mL^{-1}) in sodium phosphate solution (5 mM, pH 7.4) for 1 h, centrifuged at an RCF of 3,500 *g* for 10 min, and washed with 1 mL of sodium phosphate solution (5 mM, pH 7.4) to remove the matrix. For TEM imaging, the bacteria were fixed to a copper grid (300-mesh) using 4% paraformaldehyde in 1 mL of sodium phosphate buffer (5 mM, pH 7.4) for 1 h. The bacteria were then washed three times with 1 mL of sodium phosphate buffer (5 mM, pH 7.4) and vacuum dried for 1 h before TEM imaging.

2.5. Measurement of the membrane potentials of bacteria treated with CNGs

Bacterial membrane potentials were measured using a BacLight Membrane Potential Kit (Molecular Probes, B34950, Invitrogen). Bacterial suspensions of the wild-type and biopolymer-producing *E. coli* (10^8 CFU mL^{-1}) were treated with CNGs-270 (10 μg mL^{-1}) in 5 mM sodium phosphate solution (pH 7.4, 1 mL) at 37 °C with orbital shaking (180 rpm) for 3 h. Then, 3-chlorophenylhydrazone (CCCP, 5 μM) was added to one of the untreated bacterial suspensions as the depolarized control (positive control). Immediately after the addition of CCCP, the untreated, CCCP-treated, and CNGs-270-treated bacterial suspensions (1 mL) were incubated with $DiOC_2$ (30 μM) at room temperature for 30 min. Then, the mixtures were centrifuged (RCF 3,500 *g*, 10 min, 25 °C) and washed twice with 1X PBS to measure the bacterial membrane potentials. The green fluorescence intensities (excitation with blue light 460–480 nm) and red fluorescence (excitation with green light 510–530 nm) indicated the differences in membrane potentials in the bacteria. All bacteria exhibited green fluorescence at low concentrations of $DiOC_2$, whereas $DiOC_2$ accumulation in healthy membranes was accompanied by a shift from green to red emission due to dye stacking. The ratiometric parameter (red/green fluorescence ratio) allows for the measurement of bacterial membrane potential.

2.6. Detection of ROS induced by CNGs

The generation of intracellular reactive oxygen species (ROS) was monitored by measuring the transformation of 2′,7′-dichlorodi hydrofluorescein diacetate (DCFH-DA) to nonfluorescent 2′,7′-dic hlorodihydrofluorescein (DCFH) by cellular esterases, which was then oxidized by ROS to form the fluorescent compound 2′,7′-dic hlorofluorescein (DCF) with maximum excitation and emission wavelengths of 495 and 529 nm, respectively. Briefly, after washing (three times) with 5 mM sodium phosphate buffer (pH 7.4), wild-type and biopolymer-producing [(poly(3-hydroxybutyrate-*co*-3-hydroxyvalerate); PHBV] *E. coli* (10^8 CFU mL^{-1}) were mixed with DCFH-DA (100 μM) or sterile water only as a control. The mixtures were then incubated at 37 °C under shaking at 180 rpm for 30 min. Subsequently, CNGs-270 (100 μg mL^{-1}) or H_2O_2 (10 mM), which acted as a positive control to disrupt the cell membrane, in 5 mM sodium phosphate solution (pH 7.4) were added to the mixtures. The samples were incubated at 37 °C under a shaker at 180 rpm for 30 min. Finally, the fluorescence intensity was measured at an excitation wavelength of 488 nm. The ROS content is directly proportional to the fluorescence intensity of DCF [30].

2.7. Antimicrobial susceptibility of CNGs-270 against clinical isolates

Clinical isolates were procured from patients diagnosed with bacterial infections admitted to MacKay Memorial Hospital, Taipei, Taiwan. The sample collection protocols were in agreement with the institutional guidelines and regulations. The bacterial isolates were collected with the approval of the MacKay Memorial Hospital institutional review board (IRB-20MMHIS075e). Three gram-negative carbapenem-resistant *Acinetobacter baumannii* (CRAB) isolates from three different patients (CRAB#1, CRAB#2, and CRAB#3) and three gram-positive isolates [*methicillin-resistant Staphylococcus aureus* (MRSA) from two different patients (MRSA#1 and MRSA#2) and one patient with *Staphylococcus epidermidis* (*S. epidermidis*)] were separately incubated at 37 °C for 12 h in LB growth media. The bacterial suspensions were purified separately by centrifugation (3,000 *g*, 5 min, 37 °C) and washed three times with 1.0 mL of sodium phosphate buffer (5 mM, pH 7.4). The bacterial cultures (1×10^4 CFU mL^{-1}) were then separately incubated with CNGs or antibiotics (ampicillin, kanamycin, gentamicin, or vancomycin) at a concentration ranging from 0.1 – 100.0 μg mL^{-1} for 3 h at room temperature. Subsequently, 50 μL of each mixture was spread onto LB agar plates and then incubated at 37 °C for 18 h before CFU counting.

2.8. Drug-resistance study

The MIC values of CNGs, 30-nm silver nanoparticles (Ag NPs), gentamicin, tetracycline, vancomycin, and chlorhexidine against *E. coli* and *S. aureus* were obtained similar to Section 2.3. The MIC value of the bacteria acclimation with the mixture is obtained in the LB broth with a bacterial concentration at 10^6 CFU mL^{-1}. Three milliliters of bacteria from each test tube was diluted to 10^6 CFU mL^{-1}, and the nanomaterials or antibiotic at a concentration of half their MIC value was added. These mixtures were acclimated with the aforementioned materials at 37 °C for 24 h and new MIC values were obtained according to the protocol in Section 2.3. The test was repeated each day for 20 passages [31].

3. Results and discussion

3.1. Mild pyrolysis of L-lysine hydrochloride to form nanogel structures

CNGs were synthesized by the controlled heating of L-lysine hydrochloride in the solid state at 180, 210, 240, 270, or 300 °C for 3 h, and the samples are denoted as CNGs-180, CNGs-210, CNGs-240, CNGs-270, and CNGs-300, respectively. All the CNGs, except CNGs-300, exhibited good dispersion in aqueous solution with colors ranging from light brown to black, and their product yields were in the range of 27.5 to 98.0% (**Table S1**) due to different degrees of carbonization (**Fig. S1**). The hydrodynamic diameters of the CNGs synthesized from 180 to 270 °C showed a decrease from 604.6 to 148.8 nm (**Table S1**). During heating for 3 h, thermal polymerization of L-lysine hydrochloride tends to occur through the formation of hyperbranched polypeptide structures by dehydration and condensation followed by carbonization [32]. The carbonization of supramolecular structures increases with an increase in temperature, and the hydrodynamic diameters decrease. Heating to 300 °C caused uncontrolled carbonization, resulting in the formation of large carbon aggregates and increased hydrodynamic size (539.8 nm). The zeta (ζ) potentials of the CNGs were between + 10.0 and + 21.0 mV (**Table S1**) due to the abundant positively charged amine groups preserved on the nanogels [33]. The positive charge of the CNGs is due to the nitrogen doping and amino groups [34]. The ζ potential values showed an increasing trend from CNGs-180 to CNGs-270 due to the increased charge

density with decreasing particle size and decreased for CNGs-300 due to over-carbonization.

CNGs-180 and CNGs-210 were formed by the condensation of lysine into hyperbranched polylysine and partial carbonization [35], as seen in the transmission microscopy images (TEM, Fig. 1**A**). Notably, CNGs-240 and CNGs-270 had gel-like structures with sizes of 143.0 ± 21.4 and 120 ± 22.3 nm, respectively, from 100 counts. In contrast, large carbon aggregates with a size of 536 ± 243 nm were formed at 300 °C. The HRTEM images of the CNGs show *d*-spacings of 0.21 and 0.24 nm corresponding to the (100) and (112) lattice planes of graphite, respectively, due to the graphene-like arrangement of the carbon atoms in the CNGs (Fig. 1**B**). The CNGs exhibited strong absorption from 270 – 290 nm, which is attributed to the $\pi \rightarrow \pi^*$ transitions of conjugated C=C bonds in the as-formed graphitic nanostructures (Fig. 1**C**) [36]. The shoulder at 310–350 nm is due to the $n \rightarrow \pi^*$ transition of the functional groups with lone pair electrons, including the amino-based chromophores of the CNGs, or interlayer $\pi \rightarrow \pi^*$ charge transfer, revealing oxygen- (C=O bond) and nitrogen-containing (C=N bond) functional groups on the CNGs [37]. The CNGs also showed increasing fluorescence with increasing synthesis temperature at excitation/emission wavelengths of 365/450 nm (Fig. 1**D**) and excitation-dependent fluorescence emission (**Fig. S2**). The enhanced fluorescence of the CNGs could be due to *N*-doping-induced defective sites, surface energy traps, and improved radiative recombination of electrons and holes [38]. The polymeric structures present in the CNGs caused a crosslink-enhanced emission (CEE) effect by reducing the nonradiative transitions [39], which has not been found in other kinds of carbon dots [40]. L-lysine hydrochloride and CNGs-180, on the other hand, showed negligible fluorescence. However, the CNGs synthesized from 210 °C to 300 °C exhibited excitation-dependent fluorescence emission due to a large number of surface states [41]. The emission peak at 450 nm (CNGs-210, CNGs-240, CNGs-270, and CNGs-300 in **Fig. S2**) is due to excitation-independent behavior, suggesting the formation of a stable *N*-doped carbon core state [42,43]. The fluorescence quantum yields (QYs) of the CNGs are displayed in **Table S1,** with CNGs-300 exhibiting the highest QY (18.4%), which is probably due to the formation of a perfect carbon core state and *N*-rich surface functional groups at higher temperatures [44].

Table S1 shows the elemental compositions (*i.e.*, C, H, O, N and Cl) of the CNGs synthesized at various temperatures. The carbon content of the CNGs increased with increasing synthesis temperature (39.4–60.5%), indicating increased carbonization with temperature. In contrast, the hydrogen (7.8–8.5%), oxygen (12.5–16.3%), and nitrogen (9.6–22.1%) contents of the CNGs showed the opposite trend with temperature increase due to dehydration during the dry-heating process. Increasing halogen (chlorine) content with increasing temperature was observed in the CNGs synthesized at 180–270 °C, as determined by inductively coupled plasma mass spectrometry (ICP-MS), which increased from 16.3 to 22.0%. The material with the lowest halogen content was CNGs-300 at 4.4%. The XRD peaks of the crystalline L-lysine hydrochloride gradually decreased and disappeared with increasing synthesis temperature due to the pyrolysis of lysine (**Fig. S3**). Moreover, a broad band centered at approximately 26° (2θ) appeared in the CNGs-210 sample, corresponding to the interlayer spacing (002) in bulk graphite due to significant carbonization at this temperature. All lysine-related peaks vanished from the XRD spectra of CNGs-240, CNGs-270, and CNGs-300 due to pyrolysis, and only the peak corresponding to the interlayer spacing (002) of bulk graphite remained. The FT-IR spectra of CNGs-180 and CNGs-210 were not much different from that of L-lysine hydrochloride, revealing low carbonization at low temperatures (Fig. 1**E**). CNGs-240, CNGs-270, and CNGs-300 exhibited peaks at 2853, 2000, 1760, 1662, and 1520 cm^{-1} corresponding to C—H, C=C=N, C=O, C=C, and N—O stretching, respectively, indicating significant carbonization and oxidation of some carbon atoms at high temperatures. The C1s XPS spectra of the CNGs showed peaks at 284.0, 284.5, 285.2, 285.5, 286.7 eV, revealing C=C, C—C, C—N, C—O, and C=O bonds, respectively (**Fig. S4A**). CNGs-180 and CNGs-210 showed C1s peaks similar to those of lysine, corresponding to the XRD and FT-IR results. Notably, the C1s peaks of CNGs-240, CNGs-270, and CNGs-300 showed increasing C=C contents due to increased carbonization. The O1s XPS spectra (**Fig. S4B**) showed the presence of O=C (531.2 eV), O—H (532.2 eV), and O—C (532.8 eV) bonds, indicating hydroxyl or carboxylic groups, which provide hydrophilic features to the CNGs. The N1s XPS spectra showed C–NH–C (399.4 eV) and C=C–N (400.8 eV) bonds (**Fig. S4C**), indicating the presence of pyrrolic-N, pyridinic-N, graphitic-N, and pyridine-N oxides on the CNGs.

To understand the formation mechanism of CNGs, time-course TEM images were recorded for the dry heating of L-lysine hydrochloride at 270 °C for 10, 30, 60, 120, 180, and 240 min (**Fig. S5**). The L-lysine hydrochloride sample heated for 10 min was pale yellow, and the color deepened to dark brown and black with increasing heating time, mainly due to the carbonization of lysine. The TEM images of the products obtained after 10, 30, 60, and 120 min of heating showed bulk material that dried as a thin film, probably due to condensation of the hydroxyl, amine, and carboxylic groups to form crosslinked supramolecular-like structures several micrometers in size. Discrete 2D structures with lattice fringes were observed after heating for 180 min, suggesting that the supramolecular structures underwent significant carbonization that began at 180 min.

Constant-temperature TGA (180–300 °C) data of L-lysine hydrochloride obtained after 3 h in a preheated thermogravimetric analyzer are presented in **Fig. S6A**. Heating at 180 °C for 3 h showed<7% weight loss, probably due to the loss of moisture. Nearly 30% weight loss was observed from the samples heated from 210 – 300 °C, suggesting a higher degree of thermal decomposition with increasing temperature. Under an air atmosphere, the TGA and DSC curves in **Fig. S6B** of lysine showed a phase transition in the temperature range of 40–80 °C, which was attributed to water loss. Subsequently, the sharp exothermic peak at 230–250 °C might be a result of the initial stage of dehydration, decomposition, the condensation reaction, and the carbonization process. Then, the exothermic peak at 270–300 °C was due to decarboxylation, carbonization, and polymerization, leading to the formation of carbonized nanogels. The trivial peak observed over 300 °C might be attributed to deamination and further decomposition [45].

3.2. Broad-spectrum bactericidal activities of CNGs

Poly-L-lysine is a positively charged homopolymer with cell adhesion and antibacterial properties [46,47]. Reports have revealed that positively charged nanomaterials disrupt the integrity of the negatively charged bacterial cell membrane *via* electrostatic interactions [48]. Phosphorous-, sulfur-, and nitrogen-doped carbon dots have also been reported to exhibit antibacterial properties against drug-resistant bacteria [49]. The CNGs prepared from L-lysine hydrochloride are positively charged, partially carbonized nanogels with significant nitrogen and chlorine doping, which suggests that they may have antibacterial properties. We tested their bactericidal activity by determining their inhibition of *E. coli* and *S. aureus* using a standard dilution method (**Fig. S7**). The precursor (L-lysine hydrochloride), CNGs-180, and CNGs-210 did not show pronounced antibacterial ability even at concentrations up to 10 μg mL^{-1}. However, CNGs-240, CNGs-270, and CNGs-300 exhibited significant antibacterial activity against *E. coli* at 1.0 μg mL^{-1}. CNGs-270 and CNGs-300 showed > 99% bactericidal effects against

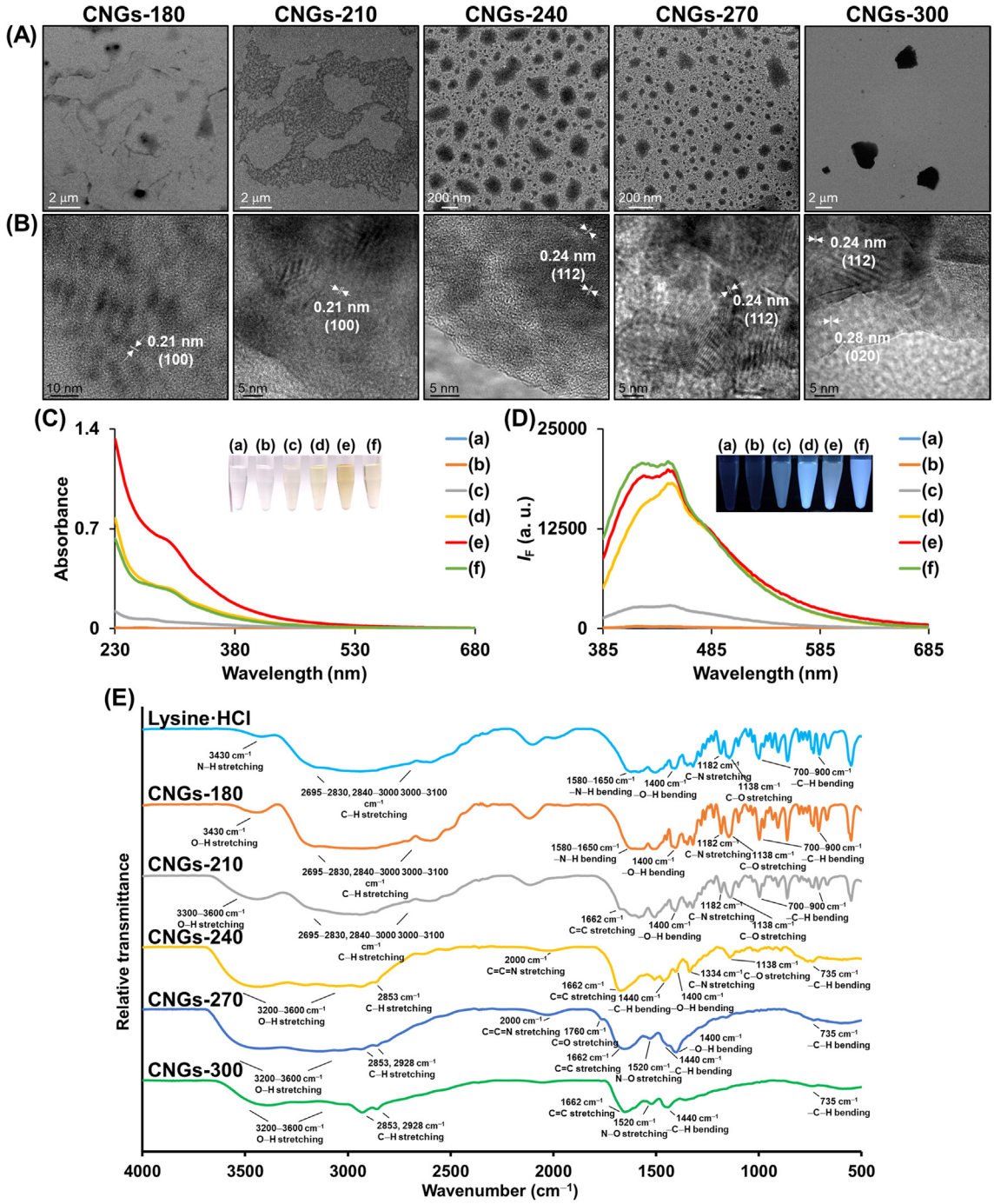

Fig. 1. The characterization of CNGs. (A) TEM and (B) HRTEM images of the as-prepared carbon nanogels from L-lysine hydrochloride. (C) UV–vis absorption and (D) fluorescence spectra of (a) L-lysine hydrochloride, (b) CNGs-180, (c) CNGs-210, (d) CNGs-240, (e) CNGs-270, and (f) CNGs-300. The concentration of all samples was 0.1 mg mL^{-1}. Insets (A) and (B) are photographs of the corresponding solutions (0.5 mg mL^{-1}) under white light and excitation with a UV lamp (365 nm), respectively. The fluorescence (I_F) intensities are plotted as arbitrary units (a. u.). (E) FT-IR spectra of L-lysine hydrochloride, CNGs-180, CNGs-210, CNGs-240, CNGs-270, and CNGs-300.

both *E. coli* and *S. aureus* at 10 μg mL^{-1}. Based on its high antibacterial activity and product yield (approximately 66.5%; **Table S1**), CNGs-270 was chosen as the optimal antibacterial material for further studies. We speculate that the strong antibacterial activity of CNGs-270 is due to its positive charge (ζ= +21.1 mV) and high surface area contact with bacterial cells. In addition, CNGs-270 has the highest chlorine content (22.0%; **Table S1**), which suggests that N and Cl co-doping in the CNGs increases both the number of defective sites and the ability to generate reactive oxygen species (ROS) *via* enhanced charge separation and charge transfer [50,51].

Recently, many studies have reported that carbon- and polymer-based nanomaterials from different precursors or metal-based nanomaterials can be used against non-multidrug-resistant (non-MDR) or even MDR pathogens [52–54]. However, to the best of our knowledge, there are no reports of antibacterial nanomaterials against biopolymer-producing bacteria, which is a serious concern due to the strong resistance of these bacteria to harsh environments and antibiotic treatments [55]. As biosynthetic polymers and plastics become mainstream products, genetically modified and highly resistant biopolymer-producing bacteria will be

used excessively by various industries [56]. However, improper handling of these bacteria may result in the transfer of high resistance genes into the environment, potentially producing highly dangerous bacterial strains. Herein, we used genetically modified *E. coli* (PHBVΔ*sdhA*) as a model biopolymer-producing bacterium for subsequent antibacterial experiments using CNGs-270 and antibacterial nanoparticles in the concentration range of 0.1 to 100 μg mL^{-1}. A typical colony-formation assay was performed with wild-type *E. coli* and biopolymer-producing *E. coli* treated with L-lysine hydrochloride, CNGs-270, silver nanoparticles (Ag NPs; 30 nm), copper oxide nanoparticles (CuO NPs; 50 nm), zinc oxide nanoparticles (ZnO NPs; 100 nm), and graphene oxide (GO; lateral size 250 nm) at a concentration of 1.0 μg mL^{-1} (Fig. 2). CNGs-270 showed superior bactericidal activity, not only against wild-type *E. coli* but also against poly(3-hydroxybutyrate-*co*-3-hydroxyvalerate) (PHBV)-producing *E. coli*. Ag NPs, which are widely used in antibacterial applications, showed negligible inhibitory effects against the biopolymer-producing *E. coli* strain. CuO NPs, ZnO NPs, and GO also showed poor inhibitory effects against both strains due to the adsorption of the biopolymers on their surfaces. Biopolymer-producing *E. coli* may exert drug-resistant activity against nanoparticles by using the biopolymer as a barrier to protect itself, which reduces nanoparticle uptake and upregulates efflux pumps [57]. Additionally, extracellular polymeric substances (EPS) are known to limit nanoparticle penetration into bacterial cells [58]. The minimum inhibitory concentration (MIC)/minimum bactericidal concentration (MBC) values of CNGs-270 for the tested bacteria were 0.6/1.3 and 1.1/2.4 μg mL^{-1} against the wild-type and biopolymer-producing strains, respectively (Table 1). In contrast, the MIC/MBC value of poly-L-lysine against biopolymer-producing *E. coli* was 392.2/498.6 μg mL^{-1} (Table 1). The MIC/MBC values of CNGs-270 toward the biopolymer-producing strain were both over 100-fold lower than those of L-lysine hydrochloride and the Ag NPs. Although metallic nanoparticles (*e.g.*, Ag NPs, CuO NPs, and ZnO NPs) are known to possess antibacterial potency, they also exhibit high cytotoxicity due to the dissolution of the metal ions (*e.g.*, Ag^{+} and Cu^{2+}) and low antimicrobial activity due to easy surface passivation by biomolecules [59]. A photopolymerized hydrogel synthesized from epsilon-poly-L-lysine-*graft*-methacrylamide was reported to exhibit antibacterial and antifungal properties and good biocompatibility; however, the MIC values were much higher than that of CNGs-270 (Table 1) [60]. Tang *et al.* reported a cationic hydrogel prepared from epoxide-polyetheramine by "click" reaction with high antibacterial and DNA binding capabilities [61]. However, in both cases, the evolution of drug resistance in bacteria was not investigated.

To elucidate the antimicrobial mechanism of CNGs-270, we employed TEM and 3,3′-diethyloxacarbocyanine iodide ($DiOC_2$) membrane potential staining on CNGs-270-treated bacteria. The TEM images showed that CNGs-270 can rupture the *E. coli*, *S. aureus*, and biopolymer-producing *E. coli* membranes. (Fig. 3**A,B**). Not even biopolymer-producing *E. coli* is resistant to CNGs-270, indicating that the biopolymer could not act as a protective agent against cell membrane damage. We speculate that CNGs-270 destabilized/dissipated the bacterial membrane and inhibited membrane synthesis probably *via* binding with phospholipids, peptidoglycans, or porins on the bacterial membrane. We used $DiOC_2$ membrane potential staining to investigate the changes in the bacterial membrane potential caused by CNGs-270 (Fig. 3**C**). The red/green fluorescence intensity ratio of *E. coli* and biopolymer-producing *E. coli* after treatment with CNGs-270 (10 μg mL^{-1}) showed a significant decrease and was similar to that of the positive control group treated with 3-chlorophenylhydrazone (CCCP) [62], indicating remarkable changes in the membrane potential. The decline in membrane potential disrupted membrane function due to the uncontrolled influx/efflux of ions and cessation of the proton gradient [63]. In addition to the bactericidal effects, we speculated that CNGs-270 could inhibit bacterial growth and cell division because the decrease in membrane potential is accompanied by the delocalization of various proteins for bacterial proliferation [64]. To further explore the antibacterial mechanism of CNGs-270, the level of ROS that causes damage to proteins, lipids, nucleic acids, and metabolites in bacteria was determined [65]. The intracellular ROS level in the wild-type and PHBV-producing *E. coli* strains remarkably increased upon exposure to CNGs-270, as revealed by DCFH-DA staining (Fig. 3**D**). The fluorescence emission intensity of the PHBV-producing strain was higher than that of the wild-type strain after treatment with CNGs-270, probably due to the biopolymer acting as a source of stress, and therefore, a higher level of ROS was produced. The ROS level of L-lysine hydrochloride, CNGs-180, CNGs-210, CNGs-240, CNGs-270, and CNGs-300 treated *E. coli* was 1.0-, 1.4-, 3.2-, 11.7-, 19.2-, and 14.4-fold higher than that of untreated ones, respectively. The positive charge on the CNGs exerts strong interaction with the bacteria resulting in elevated oxidative stress [66]. Our results suggest that the antibacterial effects of CNGs-270 are mainly due to multiple bactericidal mechanisms. In contrast to lysine, the high density of the polylysine-like structure on CNGs-270 with cationic features, a high chlorine content, a flexible shape, ROS-generating ability, and appropriate graphene-like structure caused strong interactions with the bacterial surface and severe disruption of the bacterial membrane (membrane potential of approximately − 35 mV). Therefore, the synergistic antimicrobial effects of CNGs-270 show great potential as a broad-spectrum bactericidal material.

3.3. CNGs-270 effectively inhibit clinical isolates

The antimicrobial activity of CNGs-270 was further investigated against various strains of clinical isolates, including gram-negative drug-resistant bacteria [carbapenem-resistant *Acinetobacter baumannii* (CRAB) from three different patients (CRAB#1, CRAB#2, and CRAB#3)] and gram-positive drug-resistant bacteria [*methicillin-resistant Staphylococcus aureus* (MRSA) from two different patients (MRSA#1 and MRSA#2) and *Staphylococcus epidermidis* (*S. epidermidis*) from one patient]. CRAB is a typical rod-shaped bacterium commonly found in the environment, especially in soil and water [67]. It has been identified as a perilous nosocomial pathogen that causes infection in lungs, wounds, blood, urinary tract, and other body sites and carries substantial morbidity and mortality [68]. On the other hand, gram-positive isolates such as MRSA are natural pathogenic species found mostly on the skin and thus affect burn populations; once disseminated into the bloodstream, MRSA is likely to cause nosocomial sepsis or a lung infection [69]. *S. epidermidis* can cause infection after the implantation of medical devices such as cardiac devices [70]. Fig. 4**A** shows the colony-formation assay of clinically isolated drug-resistant bacterial suspensions (1.0×10^4 CFU mL^{-1}) incubated with CNGs-270. We also investigated the effect of antibiotics on clinical isolates including aminoglycoside antibiotics (ampicillin, kanamycin, and gentamicin) and glycopeptide antibiotic (vancomycin), which are broad-spectrum antibiotics that work against many strains of gram-positive and gram-negative clinical isolates. Most clinical isolates exhibited strong drug resistance toward the above-mentioned antibiotics (MBC > 100 μg mL^{-1}). However, CNGs-270 exhibited a significant bactericidal effect against the clinical isolates (Fig. 4**B**). Notably, all clinical isolate suspensions were effectively inhibited by CNGs-270 with an MBC value of approximately 1.0–3.0 μg mL^{-1}, whereas the bactericidal effects of gentamicin against CRAB#2, MRSA#1, MRSA#2 were observed to be as high as 10 μg mL^{-1}, probably due to the restricted passage of the aminoglycosides through the cell wall. The excellent bacte-

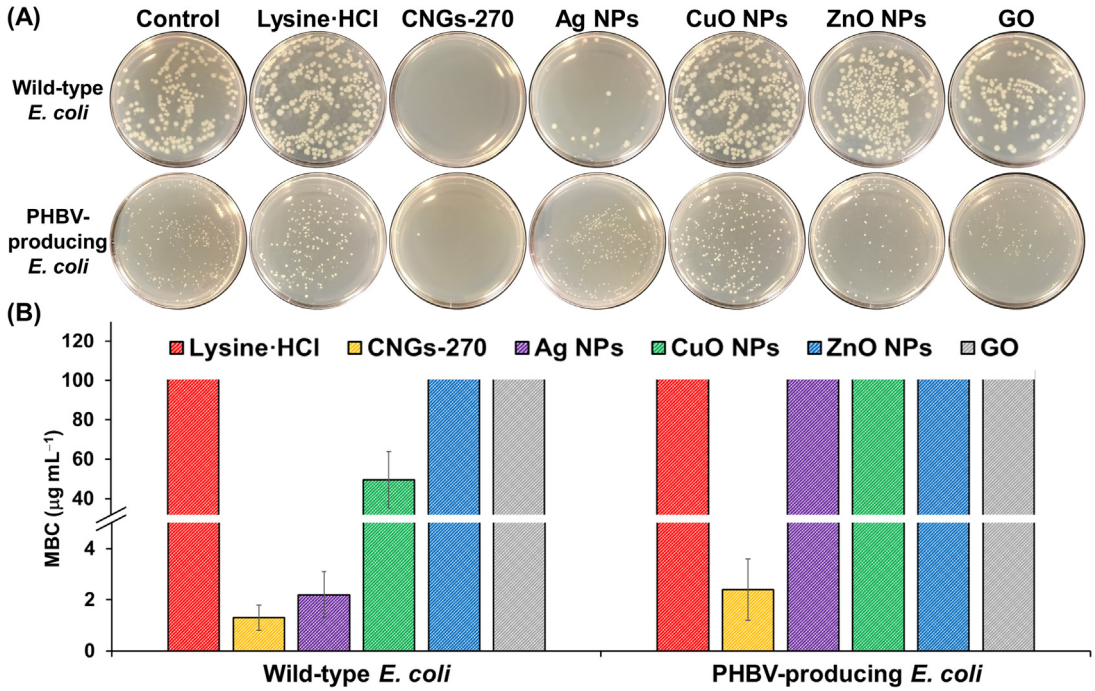

Fig. 2. (A) Representative colony formation of wild-type *E. coli* and PHBV-producing *E. coli* on LB agar plates treated separately with L-lysine hydrochloride, CNGs-270, Ag NPs, CuO NPs, ZnO NPs, and GO at 1.0 μg mL^{-1}. (B) Comparison of the MBC values of all materials against the two abovementioned strains of bacteria (n = 3).

Table 1
Minimum inhibitory concentration (MIC) and minimum bactericidal concentration (MBC) values of wild-type *E. coli* and biopolymer-producing *E. coli*.

E. coli	Wild-type		Biopolymer-producing	
Experiments	MIC[a]	MBC[a]	MIC[a]	MBC[a]
L-lysine hydrochloride	>100	>100	>100	>100
CNGs-270	0.6	1.3	1.1	2.4
Ag NPs	0.7	2.2	>100	>100
CuO NPs	23.3	49.5	87.5	>100
ZnO NPs	>100	>100	>100	>100
Graphene oxide	>100	>100	>100	>100
Poly-L-lysine	153.1	201.4	392.2	498.6

[a] Value (μg mL^{-1}) obtained from three biological replicates which showed identical results.

ricidal efficiency of CNGs-270 was mainly attributed to the aforementioned multifaceted mechanism, further supporting that CNGs-270 could be an effective antibacterial agent.

3.4. The high biocompatibility of the CNGs

To evaluate the biocompatibility of CNGs-270, the cytotoxicity and hemolysis effects in five cell lines and human red blood cells (RBCs) were evaluated. Cell toxicity assessments in the human umbilical vein endothelial cells (HUVECs), human rhabdomyosarcoma cell line (RD), human liver cancer cell line (HepG2), immortalized human keratinocyte line (HaCaT), and human embryonic kidney 293 cell line (HEK-293 T) were carried out by incubating 1–100 μg mL^{-1} CNGs-270 with the cells for 24 h and assessing cell viability using a PrestoBlue assay. CNGs-270, even at concentrations up to 100 μg mL^{-1} (approximately 100-fold the MIC value), exhibited negligible cytotoxicity toward all cell lines (Fig. 5**A**). The live/dead cell viability staining with calcein-AM/EthD-1 results in Fig. 5**B** showed that CNGs-270 (100 μg mL^{-1}) displays low cytotoxicity. The membrane potentials of the bacterial cell and mammalian cell were approximately − 35 and − 9 mV, respectively. While bacterial cells are prone to severe action by antibacterial agents, mammalian cells retain their integrity due to the higher cholesterol content in their plasma membrane [71]. Therefore, mammalian cells with a compact membrane and lower membrane potential are less susceptible to the strongly positively charged CNGs-270. Although poly-L-lysine has been reported to have great antibacterial activity and extensive applications in the industry [72], the dominating red fluorescence in the images revealed high cell toxicity at a concentration of 10 μg mL^{-1}, which was similar to ethanol treatment. An *in vitro* hemolysis assay clearly showed that CNGs-270 did not cause red blood cell rupture at a concentration of 1,000 μg mL^{-1} (Fig. 5**C**), which was approximately 1,000-fold greater than the bacterial MIC. Therefore, CNGs-270 has the potential to be a safe antibacterial agent for clinical application.

3.5. Persistent antibacterial efficacy of CNGs-270

The potential of bacteria to develop resistance to CNGs-270 and other antimicrobials, such as Ag NPs, antibiotics (gentamicin, tetracycline, and vancomycin), and bacteriostatic/bactericidal agents (chlorhexidine) after long-term antibacterial treatment was assessed. Both *E. coli* and *S. aureus* were incubated with half the MIC of the aforementioned agents each day, and the antibacterial

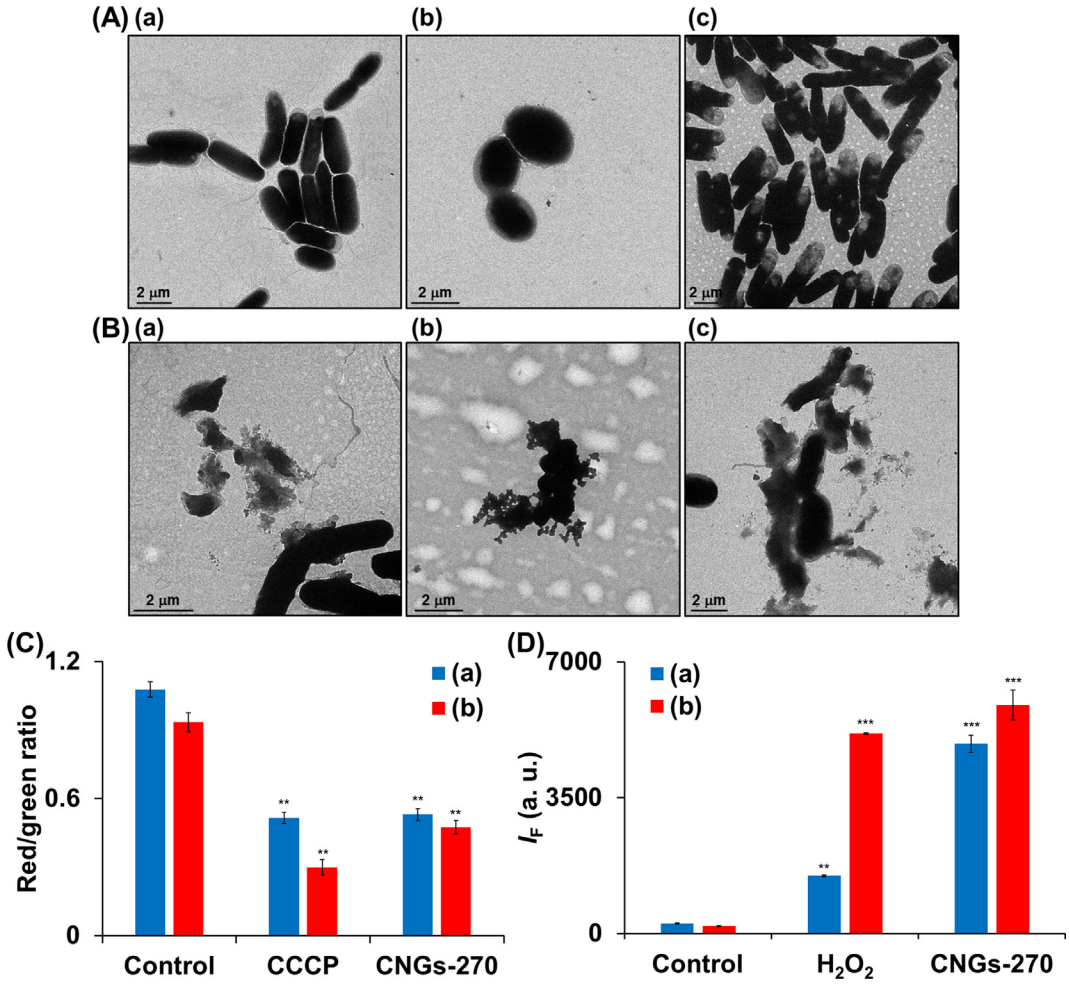

Fig. 3. The mechanism of disruption of the bacterial membrane by CNGs-270. TEM images of (a) *E. coli*, (b) *S. aureus*, and (c) PHBV-producing *E. coli* (A) before and (B) after treatment with CNGs-270 (100 μg mL^{-1}). (C) The bacterial membrane potential assay and (D) ROS assays of (a) wild-type *E. coli* and (b) PHBV-producing *E. coli* untreated (control) or treated with CNGs-270 (100 μg mL^{-1}), CCCP (5 μM) or H_2O_2 (10 mM). (**p < 0.001, ***p < 0.0001 versus control groups; n = 3).

activity was measured after the bacteria were acclimated for 20 passages. As depicted in Fig. 6**A**, the relative change in the MIC of CNGs-270 against *E. coli* and *S. aureus* were negligible even after 20 passages, which indicates that resistance toward CNGs-270 was not developed in either strain. In contrast, the MIC values after *E. coli*/*S. aureus* were treated with Ag NPs, gentamicin, tetracycline, vancomycin, and chlorhexidine increased by 3.1-/5.6-, 140.0-/5.8-, 9.8–/10.1-, 98.0-/34.9-, and 2.3-/10.6-fold, respectively. Ag NPs cause bacterial cell death by penetrating the cell wall, changing the cell membrane structure, generating ROS, and interrupting replication by releasing silver ions [73]. Reports have shown that bacteria with resistance to Ag NPs may cause aggregation of the nanoparticles by protein flagellin and genetic changes in the functions of the porins OmpF or OmpC [74]. Gentamicin inhibits bacterial protein synthesis by binding with 30S ribosomes [75]. Tetracyclines specifically inhibit the 30S ribosomal subunit, thereby preventing the binding of aminoacyl-tRNA to the acceptor site on the mRNA-ribosome complex [76]. Vancomycin, a broad-spectrum glycopeptide antibiotic against gram-positive bacteria, inhibits the synthesis of bacterial cell wall phospholipids and peptidoglycan polymerization by binding with the *N*-acyl-D-Ala-D-Ala portion. Chlorhexidine kills microbes by disrupting their cell membrane [77]. Bacteria have acquired multiple survival mechanisms to nullify the actions of antibiotics. Biofilms or biopolymers themselves provide resistance against antibiotics with mechanisms that are different from those with genetically acquired antibiotic resistance [78]. The antibiotic resistance mechanisms of bacteria include reducing antibiotic uptake through porin gene mutation, deactivating or limiting the enzyme binding of antibiotics, limiting antibiotic penetration by extracellular polymeric substances due to electrostatic repulsion, and upregulating efflux pumps to transport antibiotics [79]. Resistance to chlorhexidine, such as colistin resistance that is emerging in MDR, has resulted in numerous outbreaks and healthcare-associated infections [80]. Our results reveal that CNGs-270 did not induce the development of drug resistance. The strong physical interaction of the CNGs-270 with bacteria due to its flexible colloidal structure and positive surface charge, resulting in the disruption of the membrane function. The generation of ROS from the N- and Cl-doped CNGs-270 causes oxidative damage to the membrane and DNA of the bacteria. CNGs-270 can easily damage the cell wall without inducing bacteria to produce biochemical antibacterial mechanisms. In addition, we further examined the antibacterial activity of CNGs-270 against the drug-resistant strains obtained after 20 passages with each of the abovementioned antibacterial agents (Fig. 6**B**). The MIC values of CNGs-270 against all drug-resistant strains showed a negligible difference from that of first passage bacteria (approximately 1.0–2.3 μg mL^{-1}), which further confirms the superior antimicrobial efficacy of CNGs-270 against drug-resistant bacteria. Future research will focus on the applications and optimization of CNGs-

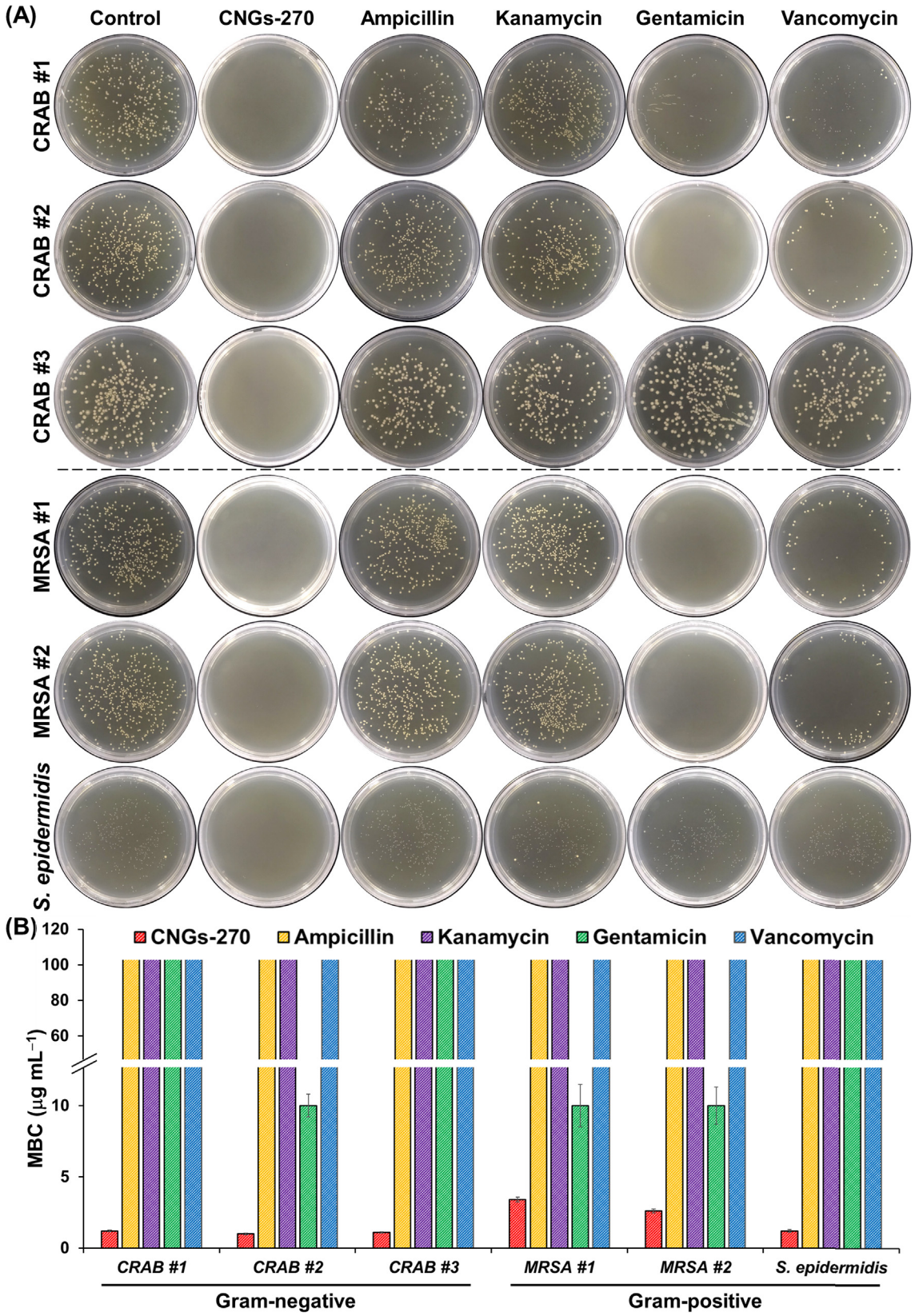

Fig. 4. (A) Representative colony formation of gram-negative and gram-positive clinical isolates treated separately with antibiotics (ampicillin, kanamycin, gentamicin, and vancomycin; 100 μg mL^{-1}) and CNGs-270 (1.0 μg mL^{-1}) dispersed in sodium phosphate buffer (5 mM, pH 7.4) and (B) comparison of the MBC values of the antibiotics and CNGs-270 against six strains of clinical isolates (n = 3).

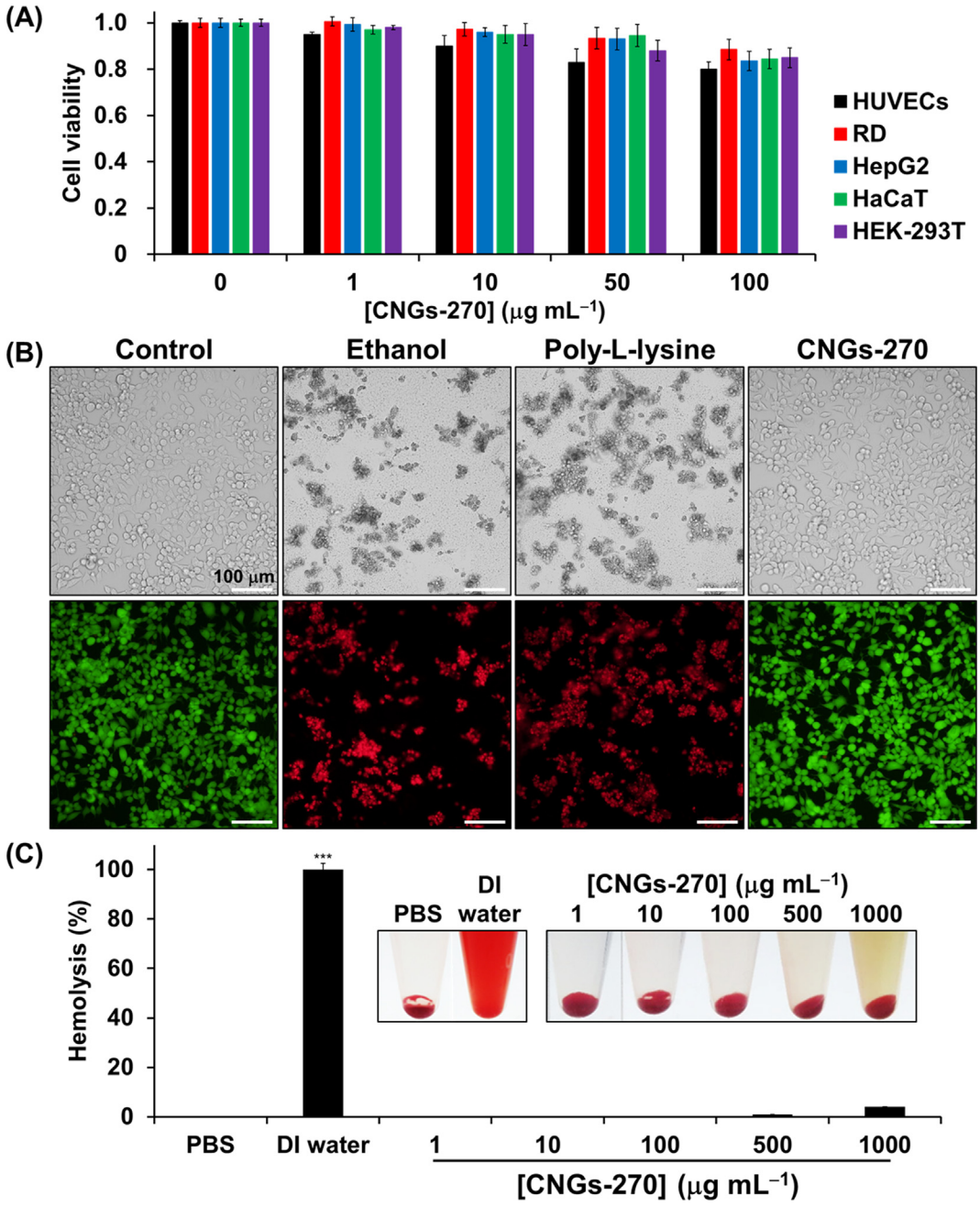

Fig. 5. Biocompatibility of CNGs-270. (A) Relative cell viability of HUVECs and RD, HepG2, HaCaT, and HEK-293 T cells incubated with CNGs-270 (1–100 μg mL^{-1}) in culture medium at 37 °C for 24 h. (B) Bright-field and fluorescent images of live/dead cell staining with calcein AM/EthD-1 in HEK-293 T cells treated with 10% ethanol (as a positive control), poly-L-lysine (10 μg mL^{-1}), and CNGs-270 (100 μg mL^{-1}) in culture medium at 37 °C for 24 h. (C) Hemolytic activity of CNGs-270 (1–1,000 μg mL^{-1}) in RBCs. PBS and DI water were used as the negative control (NC) and positive control (PC), respectively. Inset: Photographs of the corresponding RBC samples. (***$p < 0.001$ versus PBS groups; $n = 3$).

270 in animal models to demonstrate its potency in real-life clinical applications.

4. Conclusions

In summary, we have demonstrated the antibacterial activity and efficiency of lysine-derived CNGs to suppress drug resistance evolution in drug-resistant bacterial strains, clinical isolates, and biopolymer producing *E. coli*. In comparison with Ag NPs, CuO NPs, and ZnO NPs, graphene oxide, and antibiotics, CNGs-270 not only exhibited strong antibacterial activity against biopolymer-producing *E. coli* but also showed the same MIC value against bacteria acclimated to 20 generations. The results showed that CNGs-270 has a multipronged attack on resistant bacteria and strongly constrain resistance evolution. Notably, CNGs-270 exhibited superior antibacterial activity (in terms of MIC value) against the acclimated bacteria, which were resistant to Ag NPs, antibiotics (gentamicin, tetracycline, and vancomycin), and chlorhexidine. The high antibacterial activity and limited development of resistance of the CNGs-270 are mainly due to multiple antibacterial mechanisms. CNGs-270 exerts strong interaction with the bacterial membrane and elevated ROS-induced stress level, leading to membrane damage and bacterial cell death. The CNGs-270 could be reproduced and scaled-up at least 100 g per batch, showing consis-

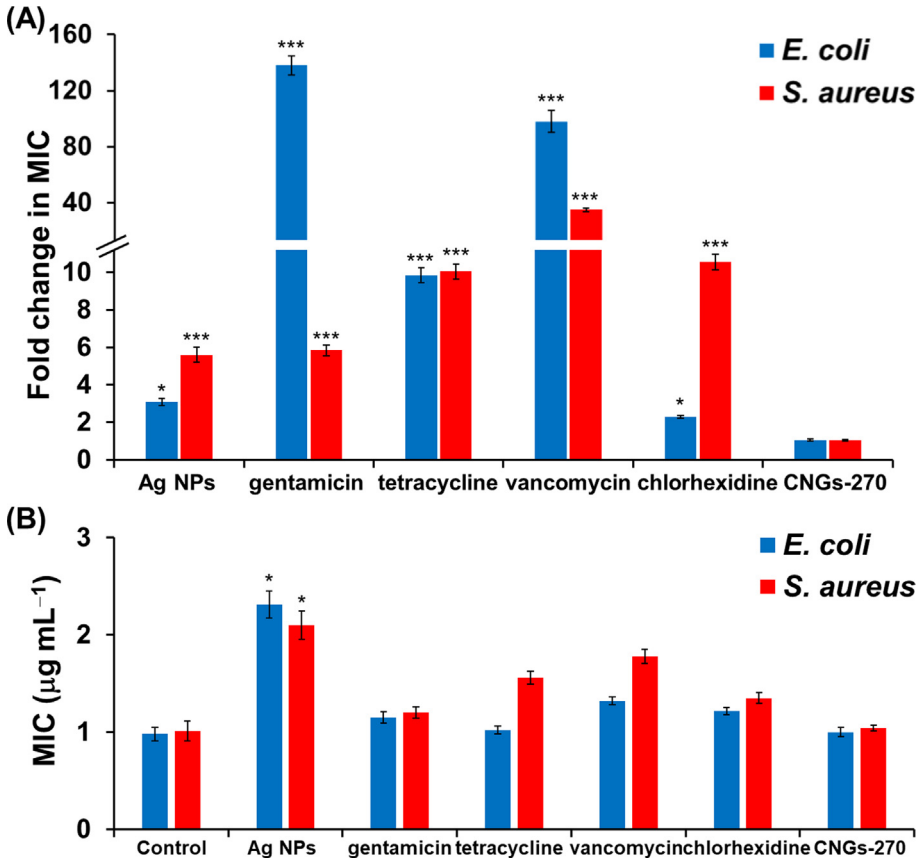

Fig. 6. Drug-resistance assay after acclimation. (A) Relative MIC values ($[MIC]_{20}/[MIC]_1$) of Ag NPs, gentamicin, tetracycline, vancomycin, chlorhexidine, and CNGs-270 against *E. coli* and *S. aureus* acclimated for 20 passages. $[MIC]_{20}$ and $[MIC]_1$ represent the MIC values at passage 20 and the first passage, respectively. (B) MIC values of CNGs-270 against the bacteria acclimated for 20 passages obtained using the aforementioned materials. ($^*p < 0.05$, $^{***}p < 0.001$ versus CNGs-270 groups; $n = 3$).

tent results and antibacterial properties. After lyophilization, the powder of CNGs-270 could be stored at room temperature for at least one year. The good reproducibility and large-scale utilization potential of CNGs-270 for industrial production could act as a novel disinfectant and antimicrobial feed additive in agriculture, animal husbandry, or aquaculture. Though CNGs derived from quercetin and lysine mixture have been reported to exhibit antibacterial properties, their ability to suppress drug resistance has not been investigated [*R*3]. Light-activated microbicidal carbon dots have been reported to be effective against bacteria, fungi, and viruses; however, different carbon dots require light with a specific wavelength and poorly visible light penetrability limit their application [R5]. In addition, their potential against drug resistance evolution in acclimated bacteria and comparison with antibiotics are rarely reported. A detailed investigation on the application of CNGs-270, a new category of carbon materials with nano-sized carbon structures embedded in the polymer matrix, for in vivo wound dressing systems, antifouling coatings on implant surfaces, tissue engineering scaffolds, and long-term toxicity will be conducted in our future work.

CRediT authorship contribution statement

Ju-Yi Mao: Investigation, Writing – original draft. **Dragan Miscevic:** Resources, Software. **Binesh Unnikrishnan:** Writing – original draft. **Han-Wei Chu:** Formal analysis, Validation. **C. Perry Chou:** Resources, Funding acquisition. **Lung Chang:** Resources. **Han-Jia Lin:** Methodology, Conceptualization, Supervision. **Chih-Ching Huang:** Conceptualization, Writing – review & editing, Project administration, Funding acquisition.

Declaration of Competing Interest

The authors declare that they have no known competing financial interests or personal relationships that could have appeared to influence the work reported in this paper.

Acknowledgments

This study was supported by the Ministry of Science and Technology of Taiwan under Contract Nos. 110-2221-E-019-001, 110-2811-M-019-501 and 110-2113-M-019-005. Thanks to Ms. C.-Y. Chien of the Ministry of Science and Technology (National Taiwan University) for assistance with the TEM experiments. The authors thank the Electron Microscopy Center of the Institute of Marine Biology at National Taiwan Ocean University for technical assistance.

Appendix A. Supplementary material

Supplementary data to this article can be found online at https://doi.org/10.1016/j.jcis.2021.10.107.

References

[1] D. Sun, K. Jeannot, Y. Xiao, C.W. Knapp, Editorial: horizontal gene transfer mediated bacterial antibiotic resistance, Front. Microbiol. 10 (2019) 1933, https://doi.org/10.3389/fmicb.2019.01933.
[2] M.A. Argudín, A. Deplano, A. Meghraoui, M. Dodémont, A. Heinrichs, O. Denis, C. Nonhoff, S. Roisin, Bacteria from animals as a pool of antimicrobial resistance genes, Antibiotics-Basel 6 (2017) 12, https://doi.org/10.3390/antibiotics6020012.

[3] P. Sedlacek, E. Slaninova, M. Koller, J. Nebesarova, I. Marova, V. Krzyzanek, S. Obruca, PHA granules help bacterial cells to preserve cell integrity when exposed to sudden osmotic imbalances, New Biotech. 49 (2019) 129–136, https://doi.org/10.1016/j.nbt.2018.10.005.
[4] E. Slaninova, P. Sedlacek, F. Mravec, L. Mullerova, O. Samek, M. Koller, O. Hesko, D. Kucera, I. Marova, S. Obruca, Light scattering on PHA granules protects bacterial cells against the harmful effects of UV radiation, Appl. Microbiol. Biotechnol. 102 (4) (2018) 1923–1931, https://doi.org/10.1007/s00253-018-8760-8.
[5] M. Koch, S. Doello, K. Gutekunst, K. Forchhammer, PHB is produced from glycogen turn-over during nitrogen starvation in *Synechocystis* sp. PCC 6803, Int. J. Mol. Sci. 20 (8) (2019) 1942, https://doi.org/10.3390/ijms20081942.
[6] D. Halet, T. Defoirdt, P. van Damme, H. Vervaeren, I. Forrez, T. van de Wiele, N. Boon, P. Sorgeloos, P. Bossier, W. Verstraete, Poly-β-hydroxybutyrate-accumulating bacteria protect gnotobiotic *Artemia franciscana* from pathogenic *Vibrio campbellii*, FEMS Microbiol. Ecol. 60 (2007) 363–369, https://doi.org/10.1111/j.1574-6941.2007.00305.x.
[7] V. Urtuvia, P. Villegas, M. González, M. Seeger, Bacterial production of the biodegradable plastics polyhydroxyalkanoates, Int. J. Biol. Macromol. 70 (2014) 208–213, https://doi.org/10.1016/j.ijbiomac.2014.06.001.
[8] M. Kumar, R. Rathour, R. Singh, Y. Sun, A. Pandey, E. Gnansounou, K.-Y. Andrew Lin, D.C.W. Tsang, I.S. Thakur, Bacterial polyhydroxyalkanoates: opportunities, challenges, and prospects, J. Clean. Prod. 263 (2020) 121500, https://doi.org/10.1016/j.jclepro.2020.121500.
[9] M.F. Moradali, B.H.A. Rehm, Bacterial biopolymers: from pathogenesis to advanced materials, Nat. Rev. Microbiol. 18 (4) (2020) 195–210, https://doi.org/10.1038/s41579-019-0313-3.
[10] D. Miscevic, J.-Y. Mao, B. Mozell, K. Srirangan, D. Abedi, M. Moo-Young, C.P. Chou, Bio-based production of poly(3-hydroxybutyrate-co-3-hydroxyvalerate) with modulated monomeric fraction in *Escherichia coli*, Appl. Microbiol. Biotechnol. 105 (4) (2021) 1435–1446, https://doi.org/10.1007/s00253-021-11108-1.
[11] D. Miscevic, J.-Y. Mao, T. Kefale, D. Abedi, C.-C. Huang, M. Moo-Young, C.P. Chou, Integrated strain engineering and bioprocessing strategies for high-level bio-based production of 3-hydroxyvalerate in *Escherichia coli*, Appl. Microbiol. Biotechnol. 104 (12) (2020) 5259–5272, https://doi.org/10.1007/s00253-020-10580-5.
[12] K. Abe, N. Nomura, S. Suzuki, Biofilms: hot spots of horizontal gene transfer (HGT) in aquatic environments, with a focus on a new HGT mechanism, FEMS Microbiol. Ecol. 96 (2020), https://doi.org/10.1093/femsec/fiaa031.
[13] Y.-T. Tan, D.J. Tillett, I.A. McKay, Molecular strategies for overcoming antibiotic resistance in bacteria, Mol. Med. Today 6 (8) (2000) 309–314, https://doi.org/10.1016/S1357-4310(00)01739-1.
[14] R. Patini, G. Mangino, L. Martellacci, G. Quaranta, L. Masucci, P. Gallenzi, The effect of different antibiotic regimens on bacterial resistance: a systematic review, Antibiotics-Basel 9 (2020) 22, https://doi.org/10.3390/antibiotics9010022.
[15] J.M.V. Makabenta, A. Nabawy, C.-H. Li, S. Schmidt-Malan, R. Patel, V.M. Rotello, Nanomaterial-based therapeutics for antibiotic-resistant bacterial infections, Nat. Rev. Microbiol. 19 (1) (2021) 23–36, https://doi.org/10.1038/s41579-020-0420-1.
[16] N. Beyth, Y. Houri-Haddad, A. Domb, W. Khan, R. Hazan, Alternative antimicrobial approach: nano-antimicrobial materials, Evid.-based Complement Altern. Med. 2015 (2015) 1–16, https://doi.org/10.1155/2015/246012.
[17] N. Durán, M. Durán, M.B. de Jesus, A.B. Seabra, W.J. Fávaro, G. Nakazato, Silver nanoparticles: a new view on mechanistic aspects on antimicrobial activity, Nanomed.-Nanotechnol, Biol. Med. 12 (3) (2016) 789–799, https://doi.org/10.1016/j.nano.2015.11.016.
[18] H. Muthukumar, N.I. Chandrasekaran, S. Naina Mohammed, S. Pichiah, M. Manickam, Iron oxide nano-material: physicochemical traits and in vitro antibacterial propensity against multidrug resistant bacteria, J. Ind. Eng. Chem. 45 (2017) 121–130, https://doi.org/10.1016/j.jiec.2016.09.014.
[19] N. Niño-Martínez, M.F. Salas Orozco, G.-A. Martínez-Castañón, F. Torres Méndez, F. Ruiz, Molecular mechanisms of bacterial resistance to metal and metal oxide nanoparticles, Int. J. Mol. Sci. 20 (11) (2019) 2808, https://doi.org/10.3390/ijms20112808.
[20] A. Panáček, L. Kvítek, M. Smékalová, R. Večeřová, M. Kolář, M. Röderová, F. Dyčka, M. Šebela, R. Prucek, O. Tomanec, R. Zbořil, Bacterial resistance to silver nanoparticles and how to overcome it, Nat. Nanotechnol. 13 (1) (2018) 65–71, https://doi.org/10.1038/s41565-017-0013-y.
[21] C. Kaweeteerawat, P. Na Ubol, S. Sangmuang, S. Aueviriyavit, R. Maniratanachote, Mechanisms of antibiotic resistance in bacteria mediated by silver nanoparticles, J. Toxicol. Environ. Health PT. A 80 (23-24) (2017) 1276–1289, https://doi.org/10.1080/15287394.2017.1376727.
[22] Q. Xin, H. Shah, A. Nawaz, W. Xie, M.Z. Akram, A. Batool, L. Tian, S.U. Jan, R. Boddula, B. Guo, Q. Liu, J.R. Gong, Antibacterial carbon-based nanomaterials, Adv. Mater. 31 (45) (2019) 1804838, https://doi.org/10.1002/adma.v31.45.
[23] B. Wang, H. Song, X. Qu, J. Chang, B. Yang, S. Lu, Carbon dots as a new class of nanomedicines: opportunities and challenges, Coord. Chem. Rev. 442 (2021) 214010, https://doi.org/10.1016/j.ccr.2021.214010.
[24] H. Li, X.u. Yan, D. Kong, R. Jin, C. Sun, D. Du, Y. Lin, G. Lu, Recent advances in carbon dots for bioimaging applications, Nanoscale Horiz. 5 (2) (2020) 218–234, https://doi.org/10.1039/C9NH00476A.
[25] Y.J. Chung, J. Kim, C.B. Park, Photonic carbon dots as an emerging nanoagent for biomedical and healthcare applications, ACS Nano 14 (6) (2020) 6470–6497, https://doi.org/10.1021/acsnano.0c02114.
[26] Q. Zeng, T. Feng, S. Tao, S. Zhu, B. Yang, Precursor-dependent structural diversity in luminescent carbonized polymer dots (CPDs): the nomenclature, Light: Sci, Appl. 10 (2021) 142, https://doi.org/10.1038/s41377-021-00579-6.
[27] J.-Y. Mao, B. Unnikrishnan, H.-W. Chu, S.G. Harroun, Y.-R. Chen, A.-T. Wu, H.-T. Chang, H.-J. Lin, C.-C. Huang, Thermally driven formation of polyphenolic carbonized nanogels with high anticoagulant activity from polysaccharides, Biomater. Sci. 9 (13) (2021) 4679–4690, https://doi.org/10.1039/D1BM00402F.
[28] H.-Y. Lin, S.-W. Wang, J.-Y. Mao, H.-T. Chang, S.G. Harroun, H.-J. Lin, C.-C. Huang, J.-Y. Lai, Carbonized nanogels for simultaneous antibacterial and antioxidant treatment of bacterial keratitis, Chem. Eng. J. 411 (2021) 128469, https://doi.org/10.1016/j.cej.2021.128469.
[29] D.-L. Chou, J.-Y. Mao, A. Anand, H.-J. Lin, J.-H.-Y. Lin, C.-P. Tseng, C.-C. Huang, H.-Y. Wang, Carbonized lysine-nanogels protect against infectious bronchitis virus, Int. J. Mol. Sci. 22 (2021) 5415, https://doi.org/10.3390/ijms22115415.
[30] X. Wang, M.G. Roper, Measurement of DCF fluorescence as a measure of reactive oxygen species in murine islets of Langerhans, Anal. Methods 6 (9) (2014) 3019–3024, https://doi.org/10.1039/C4AY00288A.
[31] A. de Breij, M. Riool, R.A. Cordfunke, N. Malanovic, L. de Boer, R.I. Koning, E. Ravensbergen, M. Franken, T. van der Heijde, B.K. Boekema, P.H.S. Kwakman, N. Kamp, A. El Ghalbzouri, K. Lohner, S.A.J. Zaat, J.W. Drijfhout, P.H. Nibbering, The antimicrobial peptide SAAP-148 combats drug-resistant bacteria and biofilms, Sci. Transl. Med. 10 (423) (2018) eaan4044, https://doi.org/10.1126/scitranslmed.aan4044.
[32] B.I. Voit, A. Lederer, Hyperbranched and highly branched polymer architectures—synthetic strategies and major characterization aspects, Chem. Rev. 109 (11) (2009) 5924–5973, https://doi.org/10.1021/cr900068q.
[33] C. Xia, S. Zhu, T. Feng, M. Yang, B. Yang, Evolution and synthesis of carbon dots: from carbon dots to carbonized polymer dots, Adv. Sci. 6 (23) (2019) 1901316, https://doi.org/10.1002/advs.v6.2310.1002/advs.201901316.
[34] N.A. Travlou, D.A. Giannakoudakis, M. Algarra, A.M. Labella, E. Rodríguez-Castellón, T.J. Bandosz, S- and N-doped carbon quantum dots: surface chemistry dependent antibacterial activity, Carbon 135 (2018) 104–111, https://doi.org/10.1016/j.carbon.2018.04.018.
[35] M. Scholl, T.Q. Nguyen, B. Bruchmann, H.-A. Klok, The thermal polymerization of amino acids revisited; Synthesis and structural characterization of hyperbranched polymers from L-lysine, J. Polym. Sci. Pol. Chem. 45 (23) (2007) 5494–5508, https://doi.org/10.1002/(ISSN)1099-0518.
[36] S. Zhu, Y. Song, X. Zhao, J. Shao, J. Zhang, B. Yang, The photoluminescence mechanism in carbon dots (graphene quantum dots, carbon nanodots, and polymer dots): current state and future perspective, Nano Res. 8 (2) (2015) 355–381, https://doi.org/10.1007/s12274-014-0644-3.
[37] Y.u. Wang, S. Kalytchuk, Y.u. Zhang, H. Shi, S.V. Kershaw, A.L. Rogach, Thickness-dependent full-color emission tunability in a flexible carbon dot ionogel, J. Phys. Chem. Lett. 5 (8) (2014) 1412–1420, https://doi.org/10.1021/jz5005335.
[38] L. Li, T. Dong, Photoluminescence tuning in carbon dots: surface passivation or/and functionalization, heteroatom doping, J. Mater. Chem. C 6 (30) (2018) 7944–7970, https://doi.org/10.1039/C7TC05878K.
[39] S. Tao, S. Lu, Y. Geng, S. Zhu, S.A.T. Redfern, Y. Song, T. Feng, W. Xu, B. Yang, Design of metal-free polymer carbon dots: a new class of room-temperature phosphorescent materials, Angew. Chem.-Int. Edit. 57 (9) (2018) 2393–2398, https://doi.org/10.1002/anie.201712662.
[40] C. Xia, S. Tao, S. Zhu, Y. Song, T. Feng, Q. Zeng, J. Liu, B. Yang, Hydrothermal addition polymerization for ultrahigh-yield carbonized polymer dots with room temperature phosphorescence via nanocomposite, Chem.-Eur. J. 24 (44) (2018) 11303–11308, https://doi.org/10.1002/chem.v24.44.
[41] M. Fu, F. Ehrat, Y.u. Wang, K.Z. Milowska, C. Reckmeier, A.L. Rogach, J.K. Stolarczyk, A.S. Urban, J. Feldmann, Carbon dots: a unique fluorescent cocktail of polycyclic aromatic hydrocarbons, Nano Lett. 15 (9) (2015) 6030–6035, https://doi.org/10.1021/acs.nanolett.5b02215.
[42] Z.-H. Wen, X.-B. Yin, Excitation-independent carbon dots, from photoluminescence mechanism to single-color application, RSC Adv. 6 (33) (2016) 27829–27835, https://doi.org/10.1039/C5RA27172J.
[43] F. Yan, Z. Sun, H. Zhang, X. Sun, Y. Jiang, Z. Bai, The fluorescence mechanism of carbon dots, and methods for tuning their emission color: a review, Microchim. Acta 186 (2019) 583, https://doi.org/10.1007/s00604-019-3688-y.
[44] H. Ding, X.-H. Li, X.-B. Chen, J.-S. Wei, X.-B. Li, H.-M. Xiong, Surface states of carbon dots and their influences on luminescence, J. Appl. Phys. 127 (23) (2020) 231101, https://doi.org/10.1063/1.5143819.
[45] F. Rodante, G. Marrosu, Thermal analysis of some α-amino acids using simultaneous TG-DSC apparatus. The use of dynamic thermogravimetry to study the chemical kinetics of solid state decomposition, Thermochim. Acta 171 171 (1990) 15–29, https://doi.org/10.1016/0040-6031(90)87002-T.
[46] M. Hyldgaard, T. Mygind, B.S. Vad, M. Stenvang, D.E. Otzen, R.L. Meyer, The antimicrobial mechanism of action of epsilon-poly-L-lysine, Appl. Environ. Microbiol. 80 (2014) 7758, https://doi.org/10.1128/AEM.02204-14.
[47] T. Yoshida, T. Nagasawa, ε-Poly-L-lysine: microbial production, biodegradation and application potential, Appl. Microbiol. Biotechnol. 62 (1) (2003) 21–26, https://doi.org/10.1007/s00253-003-1312-9.
[48] Y.N. Slavin, J. Asnis, U.O. Häfeli, H. Bach, Metal nanoparticles: understanding the mechanisms behind antibacterial activity, J. Nanobiotechnol. 15 (2017) 65, https://doi.org/10.1186/s12951-017-0308-z.

[49] C. Zhao, L. Wu, X. Wang, S. Weng, Z. Ruan, Q. Liu, L. Lin, X. Lin, Quaternary ammonium carbon quantum dots as an antimicrobial agent against gram-positive bacteria for the treatment of MRSA-infected pneumonia in mice, Carbon 163 (2020) 70–84, https://doi.org/10.1016/j.carbon.2020.03.009.
[50] L. Vallan, E.P. Urriolabeitia, F. Ruipérez, J.M. Matxain, R. Canton-Vitoria, N. Tagmatarchis, A.M. Benito, W.K. Maser, Supramolecular-enhanced charge transfer within entangled polyamide chains as the origin of the universal blue fluorescence of polymer carbon dots, J. Am. Chem. Soc. 140 (40) (2018) 12862–12869, https://doi.org/10.1021/jacs.8b0605110.1021/jacs.8b06051.s001.
[51] J. Kim, B. Pitts, P.S. Stewart, A. Camper, J. Yoon, Comparison of the antimicrobial effects of chlorine, silver ion, and tobramycin on biofilm, Antimicrob. Agents Chemother. 52 (4) (2008) 1446–1453, https://doi.org/10.1128/AAC.00054-07.
[52] X. Dong, W. Liang, M.J. Meziani, Y.-P. Sun, L. Yang, Carbon dots as potent antimicrobial agents, Theranostics 10 (2) (2020) 671–686, https://doi.org/10.7150/thno.39863.
[53] P. Makvandi, C.-y. Wang, E.N. Zare, A. Borzacchiello, L.-n. Niu, F.R. Tay, Metal-based nanomaterials in biomedical applications: antimicrobial activity and cytotoxicity aspects, Adv. Funct. Mater. 30 (22) (2020) 1910021, https://doi.org/10.1002/adfm.v30.22.
[54] B. Gómez-Gómez, L. Arregui, S. Serrano, A. Santos, T. Pérez-Corona, Y. Madrid, Selenium and tellurium-based nanoparticles as interfering factors in quorum sensing-regulated processes: violacein production and bacterial biofilm formation, Metallomics 11 (6) (2019) 1104–1114, https://doi.org/10.1039/C9MT00044E.
[55] M. Müller-Santos, J.J. Koskimäki, L.P.S. Alves, E.M. de Souza, D. Jendrossek, A.M. Pirttilä, The protective role of PHB and its degradation products against stress situations in bacteria, FEMS Microbiol. Rev. 45 (2021), https://doi.org/10.1093/femsre/fuaa058.
[56] P. Hanlon, V. Sewalt, GEMs: genetically engineered microorganisms and the regulatory oversight of their uses in modern food production, Crit. Rev. Food Sci. Nutr. 61 (6) (2021) 959–970, https://doi.org/10.1080/10408398.2020.1749026.
[57] S.C. Uzoechi, N.I. Abu-Lail, Changes in cellular elasticities and conformational properties of bacterial surface biopolymers of multidrug-resistant Escherichia coli (MDR-E. coli) strains in response to ampicillin, Cell Surf. 5 (2019) 100019, https://doi.org/10.1016/j.tcsw.2019.100019.
[58] I. Fernando, D. Lu, Y. Zhou, Interactive influence of extracellular polymeric substances (EPS) and electrolytes on the colloidal stability of silver nanoparticles, Environ. Sci.: Nano 7 7 (1) (2020) 186–197, https://doi.org/10.1039/C9EN00861F.
[59] S. Shaikh, N. Nazam, S.M.D. Rizvi, K. Ahmad, M.H. Baig, E.J. Lee, I. Choi, Mechanistic insights into the antimicrobial actions of metallic nanoparticles and their implications for multidrug resistance, Int. J. Mol. Sci. 20 (2019) 2468, https://doi.org/10.3390/ijms20102468.
[60] C. Zhou, P. Li, X. Qi, A.R.M. Sharif, Y.F. Poon, Y.e. Cao, M.W. Chang, S.S.J. Leong, M.B. Chan-Park, A photopolymerized antimicrobial hydrogel coating derived from epsilon-poly-L-lysine, Biomaterials 32 (11) (2011) 2704–2712, https://doi.org/10.1016/j.biomaterials.2010.12.040.
[61] S.C. Tang, L. Huang, R.J. Daniels-Mulholland, E. Dlugosz, E.A. Morin, S. Lenaghan, W. He, Compositional tuning of epoxide-polyetheramine "click" reaction toward cytocompatible, cationic hydrogel particles with antimicrobial and DNA binding activities, Acta Biomater. 43 (2016) 292–302, https://doi.org/10.1016/j.actbio.2016.07.011.
[62] H. Strahl, L.W. Hamoen, Membrane potential is important for bacterial cell division, Proc. Natl. Acad. Sci. U.S.A. 107 (27) (2010) 12281–12286, https://doi.org/10.1073/pnas.1005485107.
[63] J.M. Benarroch, M. Asally, The microbiologist's guide to membrane potential dynamics, Trends in Microbiology 28 (4) (2020) 304–314, https://doi.org/10.1016/j.tim.2019.12.008.
[64] N. Silber, C.L. Matos de Opitz, C. Mayer, P. Sass, Cell division protein FtsZ: from structure and mechanism to antibiotic target, Future Microbiol. 15 (9) (2020) 801–831, https://doi.org/10.2217/fmb-2019-0348.
[65] E. Cabiscol, J. Tamarit, J. Ros, Oxidative stress in bacteria and protein damage by reactive oxygen species, Int. Microbiol. 3 (2000) 3–8, https://doi.org/10.1038/nrmicro.2017.26.
[66] Y. Wu, C. Li, H.C. van der Mei, H.J. Busscher, Y. Ren, Carbon quantum dots derived from different carbon sources for antibacterial applications, Antibiotics 10 (2021) 623, https://doi.org/10.3390/antibiotics10060623.
[67] J.A. Viehman, M.-H. Nguyen, Y. Doi1, Treatment options for carbapenem-resistant and extensively drug-resistant *Acinetobacter baumannii* infections, Drugs 74 (2014) 1315–1333, https://doi.org/10.1007/s40265-014-0267-8.
[68] C.A. Moubareck, D.H. Halat, Insights into *Acinetobacter baumannii*: a review of microbiological, virulence, and resistance traits in a threatening nosocomial pathogen, Antibiotics 9 (2020) 119, https://doi.org/10.3390/antibiotics9030119.
[69] A. Hassoun, P.K. Linden, B. Friedman, Incidence, prevalence, and management of MRSA bacteremia across patient populations—a review of recent developments in MRSA management and treatment, Crit. Care 21 (2017) 211, https://doi.org/10.1186/s13054-017-1801-3.
[70] T.H. Nguyen, M.D. Park, M. Otto, Host response to *Staphylococcus epidermidis* colonization and infections, Front. Cell. Infect. Microbiol. 7 (2017) 90, https://doi.org/10.3389/fcimb.2017.00090.
[71] J. Yang, G. Gao, X. Zhang, Y.-H. Ma, X. Chen, F.-G. Wu, One-step synthesis of carbon dots with bacterial contact-enhanced fluorescence emission: fast gram-type identification and selective gram-positive bacterial inactivation, Carbon 146 (2019) 827–839, https://doi.org/10.1016/j.carbon.2019.02.040.
[72] Tuohetisayipu Tuersuntuoheti, Zhenhua Wang, Ziyuan Wang, Shan Liang, Xinping Li, Min Zhang, Review of the application of ε-poly-L-lysine in improving food quality and preservation, J. Food Process Preserv. 43 (10) (2019), https://doi.org/10.1111/jfpp.v43.1010.1111/jfpp.14153.
[73] Y. Qing, L. Cheng, R. Li, G. Liu, Y. Zhang, X. Tang, J. Wang, H. Liu, Y. Qin, Potential antibacterial mechanism of silver nanoparticles and the optimization of orthopedic implants by advanced modification technologies, Int. J. Nanomed. 13 (2018) 3311–3327, https://doi.org/10.2147/IJN.S165125.
[74] M.A. Radzig, V.A. Nadtochenko, O.A. Koksharova, J. Kiwi, V.A. Lipasova, I.A. Khmel, Antibacterial effects of silver nanoparticles on gram-negative bacteria: influence on the growth and biofilms formation, mechanisms of action, Colloid Surf. B-Biointerf. 102 (2013) 300–306, https://doi.org/10.1016/j.colsurfb.2012.07.039.
[75] Kevin M. Krause, Alisa W. Serio, Timothy R. Kane, Lynn E. Connolly, Aminoglycosides: an overview, Cold Spring Harb. Perspect. Med. 6 (6) (2016) a027029, https://doi.org/10.1101/cshperspect.a027029.
[76] Chinwe U. Chukwudi, rRNA binding sites and the molecular mechanism of action of the tetracyclines, Antimicrob. Agents Chemother. 60 (8) (2016) 4433–4441, https://doi.org/10.1128/AAC.00594-16.
[77] Hon-Yeung Cheung, Matthew Man-Kin Wong, Sau-Ha Cheung, Longman Yimin Liang, Yun-Wah Lam, Sung-Kay Chiu, Tarek Msadek, Differential actions of chlorhexidine on the cell wall of *Bacillus subtilis* and *Escherichia coli*, PLoS One 7 (5) (2012) e36659, https://doi.org/10.1371/journal.pone.0036659.
[78] D. Sharma, L. Misba, A.U. Khan, Antibiotics versus biofilm: an emerging battleground in microbial communities, Antimicrob. Resist. Infect. Control 8 (2019) 76, https://doi.org/10.1186/s13756-019-0533-3.
[79] Jose M. Munita, Cesar A. Arias, Indira T. Kudva, Qijing Zhang, Mechanisms of antibiotic resistance, Microbiol. Spectr. 4 (2) (2016), https://doi.org/10.1128/microbiolspec.VMBF-0016-2015.
[80] M.E. Wand, L.J. Bock, L.C. Bonney, J.M. Sutton, Mechanisms of increased resistance to chlorhexidine and cross-resistance to colistin following exposure of *Klebsiella pneumoniae* clinical isolates to chlorhexidine, Antimicrob. Agents Chemother. 61 (2017) e01162–e1216, https://doi.org/10.1128/AAC.01162-16.